




RESEARCH ARTICLE | FEBRUARY 19 2025

A new interaction potential for Cl^- , Li^+ , Na^+ , and Ca^{+2} in methanol solutions using the scaled charges concept

Special Collection: [Molecular Dynamics, Methods and Applications 60 Years after Rahman](#)

D. González-Salgado   ; C. Vega 



J. Chem. Phys. 162, 074502 (2025)

<https://doi.org/10.1063/5.0246314>



Articles You May Be Interested In

Freezing point depression of salt aqueous solutions using the Madrid-2019 model

J. Chem. Phys. (April 2022)

Dielectric relaxation in binary solutions: Theory and experimental results

J. Chem. Phys. (April 1998)

A modular and extensible CHARMM-compatible model for all-atom simulation of polypeptoids

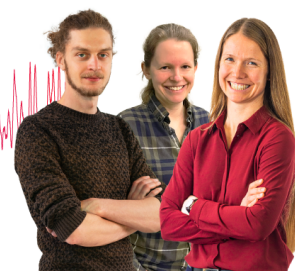
J. Chem. Phys. (December 2024)

Webinar From Noise to Knowledge

May 13th – Register now



Universität
Konstanz



A new interaction potential for Cl^- , Li^+ , Na^+ , and Ca^{+2} in methanol solutions using the scaled charges concept

Cite as: J. Chem. Phys. 162, 074502 (2025); doi: 10.1063/5.0246314

Submitted: 31 October 2024 • Accepted: 28 January 2025 •

Published Online: 19 February 2025



D. González-Salgado^{1,a)} and C. Vega²

AFFILIATIONS

¹ Departamento de Física Aplicada, Instituto de Física y Ciencias del Espacio, Universidad de Vigo, As Lagoas s/n, 32004 Ourense, Spain

² Departamento de Química Física, Facultad de Ciencias Químicas, Universidad Complutense, 28040 Madrid, Spain

Note: This paper is part of the JCP Special Topic on Molecular Dynamics, Methods and Applications 60 Years After Rahman.

a) Author to whom correspondence should be addressed: dgs@uvigo.gal

ABSTRACT

The Madrid-2019 intermolecular potential was developed for use in molecular simulations of salty aqueous solutions. The selection of the accurate TIP4P/2005 potential for water and the adoption of scaled charges for ions, $\pm 0.85e$ for monovalent ions and $\pm 1.70e$ for divalent ions, are the key features of the model. The use of scaled charges enhances the description of several properties, including solubility, transport properties, the density maximum, and the water activity in ionic solutions. In this study, we will investigate the performance of scaled charges in describing the properties of inorganic salts containing Cl^- , Li^+ , Na^+ , and Ca^{+2} in another polar solvent, methanol. The ion charges and ion–ion interactions were taken from the Madrid-2019 potential, while the accurate OPLS/2016 model was selected for methanol. The protocol used in the development of the Madrid-2019 model, particularly regarding the selection of target properties in the fitting procedure, was applied to create this potential using LiCl , NaCl , and CaCl_2 as inorganic salts. Its predictive ability was evaluated by calculating the density, dielectric constant, self-diffusion coefficients of methanol and ions, and viscosity for methanolic solutions of these three salts. As will be shown, the experimentally observed effects of salt addition are reproduced by the new model, not only qualitatively but also quantitatively. Furthermore, since the interaction potential is compatible with the Madrid-2019 model, we also demonstrated its accurate predictive ability in the ternary system methanol + water + NaCl .

Published under an exclusive license by AIP Publishing. <https://doi.org/10.1063/5.0246314>

I. INTRODUCTION

The development of intermolecular potentials for pure water to be used in molecular simulations has been extensively studied since the pioneering works of Barker and Watts¹ and Rahman and Stillinger.² The most popular potentials are rigid, non-polarizable models, due to their simplicity and accuracy. In these models, the water molecule is treated as a rigid body with a set of interaction sites located at specific positions, typically corresponding to the atomic positions. The interaction energy between sites of different molecules is generally calculated as the sum of the Lennard-Jones (LJ) intermolecular potential and a Coulombic term arising from partial charges situated at the interaction sites. Typically, a LJ site is placed at the oxygen atom of the water molecule. There are three

main approaches to the placement of charges: in three-site models such as TIP3P,³ SPC,⁴ or SPC/E,⁵ charges are located at each atom (oxygen and hydrogens); in the four-site models such as TIP4P³ or TIP4P/2005,⁶ charges are positioned on the hydrogens, with an additional charge located along the bisector of the HOH angle; and in five-site models, such as the TIP5P model,⁷ charges are placed on the hydrogens, and two negative charges represent the lone electron pairs of the oxygen. In older models, parameter values were estimated by fitting the density and vaporization enthalpy under ambient T and p conditions (i.e., 298 K and 1 bar). In more modern models, the fitting procedure has become more sophisticated, incorporating properties as a function of temperature, phase transition properties such as vapor–liquid or solid–liquid equilibrium, and singularities such as the density–temperature behavior under

ambient conditions. The TIP4P/2005 deserves special attention, as its performance has been shown to surpass that of earlier models. A comprehensive comparison of models against experimental data for a variety of properties across different phases demonstrated its superiority.⁸ This success has been attributed to an optimized charge distribution and the careful selection of target properties during the fitting procedure.

Simulations of aqueous salt solutions require the addition of electrolyte–electrolyte and water–electrolyte interaction potentials to the water–water intermolecular potential. A significant body of work has focused on developing accurate intermolecular potentials for aqueous solutions of inorganic salts.^{9–35} Notable and widely used intermolecular potentials were developed by Joung and Cheatham²¹ and the Lynden–Bell group.³⁶ In both cases, a wide variety of ions were considered; the former allows for the use of three different water models, while the latter was specifically designed for the SPC/E water model. In all these cases, monovalent electrolytes were modeled as LJ centers with charges of $+e$ for cations and $-e$ for anions. However, extensive simulations using these types of models have revealed certain deficiencies, summarized as follows: (i) The estimated viscosity and water diffusion constants at moderate concentrations are, respectively, too high and too low compared to experimental results.³⁷ (ii) The solubility of salts is significantly lower than that observed experimentally.³⁸ (iii) The number of contact ion pairs (CIPs) at moderate concentrations is too high, a phenomenon correlated with the low solubility described in point (ii). These inaccuracies have led some authors^{39–41} to consider using partial charges for ions that differ from the common $\pm e$. This approach can be theoretically justified by the fact that non-polarizable models provide an incomplete description of the electronic degrees of freedom in the simulated system. In this context, Leontyev^{42–47} proposed accounting for the effects of a phenomenological electronic continuum by scaling the ion charges by a factor of $\epsilon_{\text{el}}^{-1/2}$, where ϵ_{el} is the experimental high-frequency dielectric constant of pure water.⁴⁸ With this adjustment, the scaled partial charges for the ions became $\pm 0.75e$. This approach was adopted by Jungwirth and co-workers^{49–53} to develop an improved intermolecular potential for salty aqueous solutions. On the other hand, Kann and Skinner⁵⁴ suggested setting $\epsilon_{\text{el}} = \epsilon_{\text{exp}}/\epsilon_{\text{sim}}$, i.e., the ratio between the experimental and simulated dielectric constants of pure water. This method has the advantage of recovering the Debye–Hückel law at infinite dilution. Vega and co-workers^{39,55} applied Skinner’s suggestion along with the accurate TIP4P/2005 water model and a specific fitting methodology to develop an improved intermolecular potential for salty aqueous solutions: the Madrid-2019 model. In this model, the partial charges for monovalent ions were set to $\pm 0.85e$ and for divalent ions to $\pm 1.70e$.

The methanol molecule can be derived from water by substituting one hydrogen atom with a methyl group. This simple modification induces significant changes at the molecular scale (e.g., the tetrahedral network of pure water disappears, and linear chains become the preferred aggregates) and in thermodynamic behavior, where most of the anomalies observed in pure water are absent in methanol. In the simplest rigid, non-polarizable models, methanol is typically represented as a three-site model, with both a LJ center and a partial charge assigned to the methyl group and the oxygen atom, while the hydrogen atom is modeled with a single partial charge. As with water models, the initial parameterizations for

methanol models were based on fitting to properties such as density and vaporization enthalpy. Notable examples include the OPLS model by Jorgensen⁵⁶ and the H1 model by Haughney *et al.*⁵⁷ Subsequent improvements incorporated additional properties, such as vapor–liquid equilibrium (VLE) data, into the fitting process, as shown in the L1⁵⁸ and L2⁵⁹ models. The OPLS/2016 model⁶⁰ is considered the methanol equivalent of the TIP4P/2005 model for water. Its parameterization was derived using the same fitting methodology as TIP4P/2005 and provides the most accurate description of methanol, as demonstrated in extensive comparisons with experimental data (these include dynamic and thermodynamic properties, as well as phase change thermodynamics⁶⁰). Simulations of salty methanolic solutions have often used salt parameterizations originally developed for aqueous solutions. These typically involve the LJ parameters and partial charges for the ions defined in those studies, combined with selected combining rules for cross LJ parameters between methanol sites and ions.^{61–69} For specific salts in methanolic solutions, tailored interaction parameters have been proposed.^{70–73} In all cases, the partial charges of the ions were set to $\pm e$ for monovalent ions and $\pm 2e$ for divalent ions.

Developing an intermolecular potential for salty methanolic solutions using the accurate OPLS/2016 model for methanol and LJ centers with scaled charges for ions appears to be a natural improvement in this field. According to the scaling method proposed by Skinner, the scaling factor for this model is 0.91. While this value would result in the most accurate potential for methanolic salty solutions, it presents a significant disadvantage: it is incompatible with the Madrid-2019 model. Consequently, ternary systems involving methanol, water, and salts could not be studied. Since 0.91 is relatively close to 0.85, we believe it is preferable to ensure compatibility by accepting a slight degree of inaccuracy. Therefore, the new potential should adopt the same scaled charges as the Madrid-2019 model ($\pm 0.85e$ for monovalent ions and $\pm 1.70e$ for divalent ions), as well as identical ion–ion interactions.

In this work, we initiated the development of this potential by determining the interactions between the sites of the OPLS/2016 methanol model and the ions Cl^- , Li^+ , Na^+ , and Ca^{+2} . The same fitting methodology used in the development of the Madrid-2019 model was applied here, utilizing reference data for methanolic solutions of two monovalent salts (sodium chloride, NaCl; and lithium chloride, LiCl) and one divalent salt (calcium chloride, CaCl_2). The predictive ability of the new potential was evaluated by calculating the density, self-diffusion coefficients for methanol and ions, the dielectric constant, and viscosity, which were then compared with the available experimental data for the selected methanolic solutions. Finally, based on the claimed compatibility, we combined this new potential with the Madrid-2019 model to test its accuracy in the ternary methanol + water + NaCl system. Salty solutions in the water + methanol system have garnered considerable attention in recent years.^{67,74–85}

II. MODELS AND SIMULATION DETAILS

The OPLS/2016 model treats methanol as a rigid body with three mass centers located in the methyl group (CH_3), the oxygen atom of the hydroxyl group (O_M), and the hydrogen atom of the hydroxyl group (H). Both the methyl group and the oxygen atom serve as LJ centers and carry partial charges, while the

TABLE I. Lennard-Jones parameters, ϵ_a and σ_a ; partial charges, q_a ; and geometry of the OPLS/2016 model for methanol, TIP4P/2005 model for water, and Madrid-2019 for ions Cl^- , Li^+ , Na^+ , and Ca^{+2} .

	ϵ_a (kJ mol ⁻¹)	σ_a (nm)	q_a (e)	Geometry
OPLS/2016				
CH ₃	0.918 333 2	0.364 99	0.1546	d (O-CH ₃) = 0.143 nm
O _M	0.812 947 3	0.316 59	-0.6544	d (O-H) = 0.0945 nm
H	0.0	0.0	0.4998	H-O-CH ₃ = 108.50°
TIP4P/2005				
O _W	0.774 90	0.315 89	0.0	d (O _W -H _{W1}) = 0.095 72 nm
H _{W1}	0.0	0.0	0.5564	d (O _W -H _{W2}) = 0.095 72 nm
H _{W2}	0.0	0.0	0.5564	d (O _W -M) = 0.015 46 nm
M			-1.1128	H _{W1} -O _W -H _{W2} = 104.52°
Madrid-2019				
Cl ⁻	0.076 923 08	0.469 905 63	-0.85	
Li ⁺	0.435 090	0.143 970	0.85	
Na ⁺	1.472 355 77	0.221 736 68	0.85	
Ca ⁺²	0.507 200	0.266 560	1.70	

hydrogen atom only carries a partial charge. Table I provides the values of the LJ parameters, partial charges, and molecular geometry for methanol. The Madrid-2019 model was employed to represent the ions Cl^- , Li^+ , Na^+ , and Ca^{+2} . In this model, the ions are represented as LJ centers with partial charges of $\pm 0.85e$ for monovalent ions and $\pm 1.70e$ for divalent ions. The parameters for each ion in the Madrid-2019 model are also listed in Table I.

The intermolecular energy U_{ab} between sites a and b of different molecules or ions is evaluated from the following function:

$$U_{ab} = 4\epsilon_{ab} \left(\left(\frac{\sigma_{ab}}{r_{ab}} \right)^{12} - \left(\frac{\sigma_{ab}}{r_{ab}} \right)^6 \right) + \frac{1}{4\pi\epsilon_0} \frac{q_a q_b}{r_{ab}}, \quad (1)$$

where ϵ_{ab} and σ_{ab} are the LJ cross parameters between a and b sites, r_{ab} is the distance between sites, q_a and q_b are the charges of both

sites, and ϵ_0 is the relative permittivity of vacuum. Partial charges are presented in Table I. The LJ cross parameters between the same interaction sites in different molecules or ions are those given in Table I. The LJ cross parameters between distinct interaction sites, ϵ_{ab} and σ_{ab} , involved in methanol-methanol, methanol-ion, and ion-ion interactions are now established. The LJ cross parameters for methanol-methanol interactions are calculated using the geometric mean combining rule [$\epsilon_{ab} = (\epsilon_a \epsilon_b)^{1/2}$; $\sigma_{ab} = (\sigma_a \sigma_b)^{1/2}$]. These parameters are derived from the LJ parameters listed in Table I. The ion-ion LJ cross parameters were taken from the Madrid-2019 model, which in some cases employs the Lorentz-Berthelot (LB) combining rule: [$\epsilon_{ab} = (\epsilon_a \epsilon_b)^{1/2}$; $\sigma_{ab} = (\sigma_a + \sigma_b)/2$]. Finally, the LJ cross parameters for methanol-ion interactions, which represent the novelty of this work, are determined following the fitting procedure described below. All the resulting parameters are provided in Tables II and III.

TABLE II. Epsilon cross Lennard-Jones parameter, ϵ_{ab} , between sites of different molecules or ions. In bold are highlighted the fitted parameters of this work not derived from any combining rule, and in plain text, the parameters obtained using both the geometric mean or the Lorentz-Berthelot combining rules (from the LJ parameter of each site given in Table I) or the values taken from the Madrid-2019 force field.

	ϵ_{ab} (kJ mol ⁻¹)					
Site/site	O _M	O _W	Cl ⁻	Li ⁺	Na ⁺	Ca ⁺²
CH ₃	0.864 035 01 ^a	1.207 385 8 ^b	0.265 783 78 ^c	7.5	7.2	9.5
O _M		0.712 159 3 ^b	0.250 068 81 ^c	7.5	7.2	9.5
O _W			0.061 983 47 ^d	0.700 650 03 ^d	0.793 388 30 ^d	7.25 ^d
Cl ⁻				1.282 943 85 ^d	1.438 894 23 ^d	1.00 ^d

^aGeometric mean combining rule.

^bGonzález-Salgado *et al.*⁸⁶

^cLorentz-Berthelot combining rule.

^dMadrid-2019 model.

TABLE III. Sigma cross Lennard-Jones parameter, σ_{ab} , between different sites or different molecules or ions. In bold are highlighted the fitted parameters of this work not derived from any combining rule, and in plain text, the parameters obtained using both the geometric mean or the Lorentz–Berthelot combining rules (from the LJ parameter of each site given in Table I) or the values taken from the Madrid-2019 force field.

Site/site	σ_{ab} (nm)					
	O _M	O _W	Cl [−]	Li ⁺	Na ⁺	Ca ⁺²
CH ₃	0.339 929 68 ^a	0.340 06 ^b	0.417 447 82 ^c	0.254 48 ^c	0.293 363 34 ^c	0.215 775
O _M		0.317 93 ^b	0.393 247 82 ^c	0.230 28 ^c	0.269 163 34 ^c	0.191 575
O _W			0.423 866 98 ^d	0.212 000 00 ^d	0.260 837 54 ^d	0.240 000 00 ^d
Cl [−]				0.270 000 00 ^d	0.300 512 31 ^d	0.315 000 00 ^d

^aGeometric mean combining rule.

^bGonzález-Salgado *et al.*⁸⁶

^cLorentz–Berthelot combining rule.

^dMadrid-2019 model.

In this work, we adopt the same fitting approach proposed for the development of the Madrid-2019 model. In particular, it is necessary to determine only the LJ cross parameters between the CH₃ and O_M sites in the OPLS/2016 model and the ions Cl[−], Li⁺, Na⁺, and Ca⁺². The total number of parameters to be determined is 16. The LJ cross parameters were optimized by using the experimental density of methanolic solutions of the salts NaCl, LiCl, and CaCl₂ as the target property in the fitting procedure. Density was chosen as the target property, as in the development of the Madrid-2019 model, due to its reliable and high-accuracy experimental measurements. In addition, we monitored the number of contact ion pairs (CIPs) at the solubility limit, ensuring low values to prevent precipitation at low concentrations. This approach is based on the findings of Benavides *et al.*,⁸⁷ who demonstrated that CIP values lower than 0.5 in aqueous solutions with solubility below 11 m ensure homogeneous mixing at the experimental solubility.

Initially, we tested whether the densities of our systems could be accurately predicted while keeping all parameters fixed to the values determined by the LB combining rule. As shown below, this approach consistently underestimated the experimental densities. To define a new set of parameter values in a straightforward manner, we decided to constrain most of the parameters to the LB values, allowing only a few to vary during the optimization process. Our initial decision was to constrain the anion–methanol interaction, as the σ values determined by the LB combining rule closely agree (as will be shown below) with the experimental position of the maximum in the anion–methanol radial distribution function. With this choice, the responsibility for fitting was placed entirely on the cation–methanol interaction. A priori, an increase in density could be achieved either by decreasing the σ parameter or by increasing the ϵ parameter. To simplify the process, we considered the same ϵ value for the cation–CH₃ and cation–O_M interactions and avoided simultaneous variation of both σ and ϵ parameters. After testing both approaches, we found better performance by increasing the ϵ parameters for the cation–methanol interactions in the NaCl and LiCl solutions (this result is illustrated in the [supplementary material](#) for LiCl solutions). In the case of CaCl₂, while the density could also be accurately predicted using this scheme, the CIP value at the solubility limit was too high. Consequently, we opted to

also reduce the σ values for the cation–methanol interaction. This adjustment yielded a set of parameters that met all the requirements of the proposed protocol. As will be shown, this reduction allowed our simulations to match the experimental position of the maximum in the cation–methanol radial distribution function. In summary, we assumed the following: (i) the LJ cross parameters (anion–methanol), ϵ_{ab} and σ_{ab} , for Cl[−], and the σ_{ab} values (cation–methanol) for Li⁺ and Na⁺ were fixed by the LB combining rule; and (ii) the ϵ_{ab} parameters for cation interactions with CH₃ and O_M were the same. With these considerations, the number of fitting variables was reduced to five. As shown in Table II, the ϵ parameters for cation–methanol interactions are an order of magnitude higher than the LB values. This result stems primarily from the constraints imposed during the fitting procedure, although other approaches could yield similar results at the cost of increased complexity in the fitting process.

NVT and NpT molecular dynamics simulations^{88,89} were performed using the GROMACS software (2021 version)⁹⁰ using a cubic box under periodic boundary conditions. The Nosé–Hoover thermostat^{91,92} and the Parrinello–Rahman barostat⁹³ were chosen to fix temperature and pressure using, in both cases, 2 ps as a time constant. Equations of motion were integrated using the Verlet algorithm with a time constant of 1 fs. A cutoff radius of 1 nm was used to compute the Lennard-Jones interaction, and it was also used for the real part of the Particle Mesh Ewald method⁹⁴ (PME), which was selected for dealing with Coulombic interactions. The non-real part of the PME method was evaluated with a fourth degree interpolation and a mesh size of 0.1 nm. Common long range corrections to energy and pressure for the Lennard-Jones part of the potential were included.⁸⁸ The lengths of the simulations were typically 10 ns for NpT and 200 ns for NVT simulations.

NpT simulations were used for computing the density and the radial distribution functions (rdf). From the radial distribution function between sites X and Y, $g_{XY}(r)$, we have computed the number $n_{Y(X)}$ of atoms/groups Y in the first coordination shell of site X using the following expression:

$$n_{Y(X)} = \int_0^{r_{\min}} dr 4\pi r^2 g_{XY}(r) \rho_Y, \quad (2)$$

where r is the distance between X and Y sites, r_{\min} is the position of the first minimum in the rdf, and ρ_Y is the number density of Y sites in the system. When X and Y are a cation and an anion, respectively, $n_{Y(X)}$ is the number of ionic contact pairs, CIP, and when X is an ion and Y is the oxygen atom in methanol, $n_{Y(X)}$ is the number of coordination of ion X .

NVT simulations were employed for the evaluation of the dielectric constant, diffusion coefficient for ions and methanol, and the shear viscosity. Configurations were stored every 100 simulation steps for the calculation of the first two magnitudes. The dielectric constant, ϵ , is evaluated using the following formula:

$$\epsilon = 1 + \frac{4\pi}{3kTV} \langle M^2 \rangle, \quad (3)$$

where k is the Boltzmann constant, T is the temperature, V is the volume, and M is the total dipolar moment in the simulation box. The self-diffusion coefficient, D , was evaluated using the following Einstein equation:

$$6Dt = \lim_{t \rightarrow \infty} \langle |\mathbf{r}_i(t) - \mathbf{r}_i(0)|^2 \rangle, \quad (4)$$

where $\mathbf{r}_i(t)$ is the vector of the position of particle i at time t . The 100–500 ps window was considered for our calculations. The shear viscosity, η , was evaluated through the Green–Kubo relation,

$$\eta = \frac{V}{kT} \int_0^\infty dt \langle P_{\alpha\beta}(t_0) P_{\alpha\beta}(t_0 + t) \rangle, \quad (5)$$

where $P_{\alpha\beta}$ is the component $\alpha\beta$ (off-diagonal) of the pressure tensor, and the brackets represent an average over different time origins. We have computed the average for the off-diagonal components P_{xy} , P_{xz} , and P_{yz} , but also for $(P_{xx} - P_{yy})/2$ and $(P_{yy} - P_{zz})/2$. Since all of them are mutually equivalent, the final autocorrelation function, ACF, was computed as the average of all these results. Finally, the shear viscosity was determined by integration of ACF up to 60 ps in all the cases except in the highest salt mole fractions of the CaCl_2 system, for which 240 ps were needed.

III. RESULTS AND DISCUSSION

The concentration of each mixture is characterized by the salt mole fraction, defined here as $x = N_+ / (N_+ + N_{\text{met}})$, where N_+ is the number of cations and N_{met} is the number of methanol molecules.

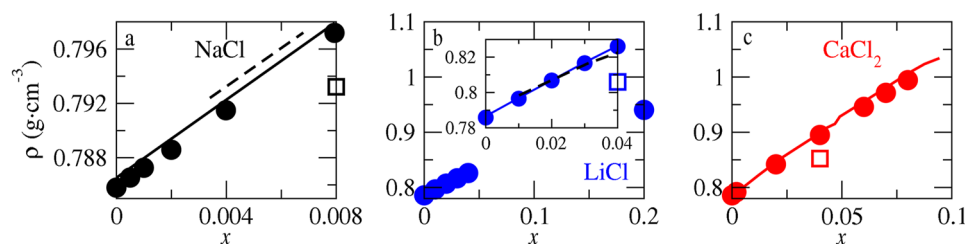


FIG. 1. Density, ρ , plotted against salt mole fraction, x , at 298.15 K and 1 bar for methanolic solutions of (a) NaCl (black), (b) LiCl (blue), and (c) CaCl_2 (red). Empty squares (results obtained by using Lorentz–Berthelot combining rules for methanol–ion interactions, OPLS/2016 for methanol–methanol interactions, and the Madrid-2019 force field for ion–ion interactions), dotted lines (results obtained with the force field proposed by Reiser *et al.*⁶⁴), and filled circles (simulation results obtained with the force field proposed in this work). Full lines are experimental data. The inset graphic expands the region where simulation data can be compared with experimental data for LiCl solutions, which are available only up to a molar fraction of 0.04.

TABLE IV. Number of methanol molecules, N_{met} , of cations, N_+ , and anions, N_- , for the salty methanol solutions of salt mole fraction, x .

Salt	x	N_{met}	N_-	N_+
NaCl	0.000 499	4000	2	2
NaCl	0.000 999	4000	4	4
NaCl	0.001 996	4000	8	8
NaCl	0.003 984	4000	16	16
NaCl	0.007 936	4000	32	32
LiCl	0.001 996	4000	8	8
LiCl	0.010 146	4000	41	41
LiCl	0.020 088	4000	82	82
LiCl	0.030 068	4000	124	124
LiCl	0.040 077	4000	167	167
LiCl	0.20	3200	800	800
CaCl_2	0.001 996	4000	16	8
CaCl_2	0.020 088	4000	164	82
CaCl_2	0.040 077	4000	334	167
CaCl_2	0.059 929	4000	510	255
CaCl_2	0.069 984	4000	602	301
CaCl_2	0.080 037	4000	696	348

All simulations were performed at 298.15 K and 1 bar. At room temperature and pressure, the solubility of NaCl in methanol, expressed as the mole fraction (the ratio of the number of moles of salt to the total number of moles in the mixture), is significantly lower ($x = 0.008$)⁹⁵ compared to LiCl ($x = 0.25$)⁹⁶ and CaCl_2 ($x = 0.10$).⁹⁷ All simulations were conducted with $N_{\text{met}} = 4000$, except for one mixture where $N_{\text{met}} = 3200$. This choice ensures that finite-size effects (especially for diffusion coefficients that typically increase with the system size⁹⁸) should be quite small while allowing simulations with enough numbers of ions within the composition range where NaCl is soluble. Table IV provides the specific values of the number of methanol molecules, N_{met} , anions, N_- , and cations, N_+ , used in the simulated mixtures.

Figures 1–7 present the density, ρ ; dielectric constant, ϵ ; viscosity, η ; self-diffusion coefficients, D_{met} , D_{Cl} , and D_i , where i represents Na^+ , Li^+ , or Ca^{+2} ; as well as several derived properties, plotted as a function of salt mole fraction, x , compared with the available experimental data. Where available, simulation data from Reiser *et al.*⁶⁴

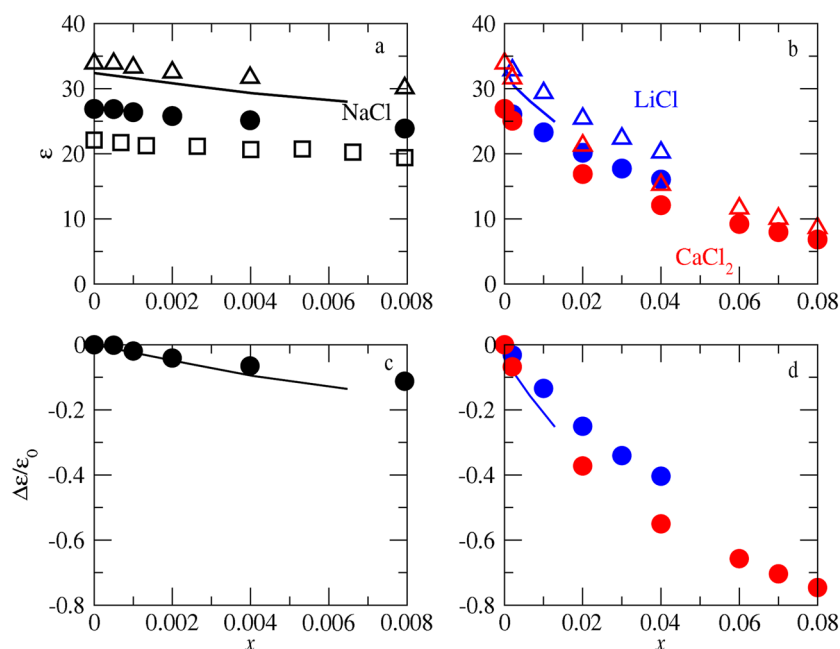


FIG. 2. (a) and (b) Dielectric constant, ϵ , and (c) and (d) $\Delta\epsilon = (\epsilon(x) - \epsilon(0))/\epsilon(0)$ plotted against salt mole fraction, x , at 298.15 K and 1 bar for methanolic solutions of NaCl (black), LiCl (blue), and CaCl₂ (red). Full circles are the simulation data of this work, empty squares are the simulation data of the Reiser *et al.*⁶⁴ model reported by Pizio and co-workers,⁹⁹ and full lines are the experimental data. Empty triangles are the simulation data of this work corrected by the factor 1.26.

and Pizio and co-workers⁹⁹ are included in order to compare our results with a parameterization that uses the L2⁵⁹ model for methanol and charges $\pm e$ for monovalent salts and $\pm 2e$ for divalent salts. In Fig. 1, simulation data obtained using the LB combining rule are also included to emphasize the importance of conducting a new parameterization. Except for Fig. 1, all other figures are organized into two columns: the left column shows results for methanolic solutions of NaCl, while the right column presents results for solutions of LiCl and CaCl₂. This layout was chosen to improve clarity due to the limited solubility of NaCl in methanol.

The simulated density is presented in Fig. 1 alongside experimental data.^{64,100,101} Starting with the NaCl methanolic solution [Fig. 1(a)], it is worth noting that the simulation data at $x = 0$ (pure methanol) is slightly lower than the experimental value. This discrepancy arises solely from the OPLS/2016 model and was maintained approximately constant during the fitting process to ensure that the new parameterization accurately captures the experimental variation in density with the addition of salt. Consequently, the

experimental ρ - x slope (1.43 g cm^{-3}) is in excellent agreement with the simulated slope (1.43 g cm^{-3}). A similar approach was applied to the methanolic solutions of LiCl and CaCl₂, as shown in Figs. 1(b) and 1(c). The agreement between experimental and simulation data is evident, and the deviation observed at $x = 0$ in NaCl is not appreciated here due to the larger range in both axes. The experimental and simulated ρ - x slopes for LiCl are ($1.04, 1.05 \text{ g cm}^{-3}$), and for CaCl₂ are ($2.67, 2.64 \text{ g cm}^{-3}$). These results clearly rank the effect of salt addition on density as $\text{LiCl} < \text{NaCl} < \text{CaCl}_2$. Furthermore, simulation data from Reiser *et al.*⁶⁴ also show good agreement with simulation results (although overestimating the experimental densities slightly for NaCl solutions and underestimating them for LiCl solutions at high concentrations).

The simulated dielectric constant for the salty methanolic solutions of this work is presented in Figs. 2(a) and 2(b) compared to experimental data.¹⁰² Experimental data are only available for NaCl and LiCl solutions. In the salt mole fraction range $x = 0$ – 0.010 , where the two monovalent salt solutions (NaCl and LiCl) can be directly

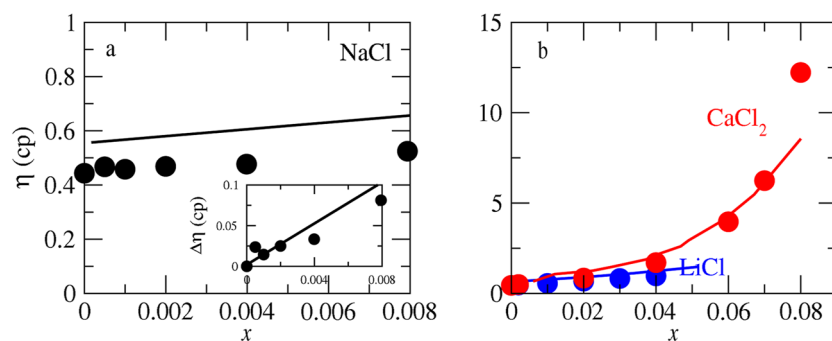


FIG. 3. Shear viscosity, η , plotted against salt mole fraction, x , at 298.15 K and 1 bar for methanolic solutions of (a) NaCl (black), (b) LiCl (blue), and CaCl₂ (red). Points are simulation data, and full lines are experimental data. In the inset graphic, $\Delta\eta = \eta(x) - \eta(0)$ is plotted vs salt mole fraction, x , for methanolic solutions of NaCl. This inset figure eliminates the small deficiency of the OPLS/2016 model to predict the viscosity of pure methanol.

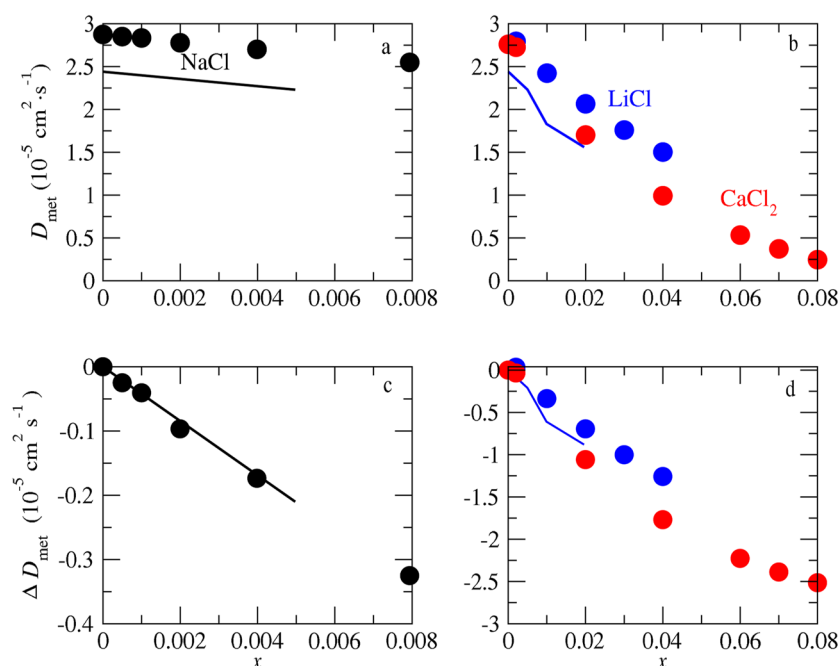


FIG. 4. (a) and (b) Self-diffusion coefficient, D_{met} , of methanol and (c) and (d) $\Delta D_{\text{met}} = D_{\text{met}}(x) - D_{\text{met}}(0)$ plotted against salt mole fraction, x , at 298.15 K and 1 bar for methanolic solutions of NaCl (black), LiCl (blue), and CaCl₂ (red). Points are the simulation data, and full lines are the experimental data.

compared, no significant differences were observed between both simulation data. For CaCl₂ solutions, the simulated results are very close to those of LiCl, although with slightly lower values. It is worth noting that the dielectric constant for pure methanol predicted by the OPLS/2016 model is slightly lower than the experimental value. This discrepancy should not be viewed as a deficiency of the model. As previously discussed, models that accurately predict the dielectric constant often perform poorly in other properties, whereas those with better overall performance typically fail to reproduce this property precisely. This point was extensively discussed by one of us in previous contributions.^{103,104} To address this, Jorge and Lue⁴⁰ proposed including polarization effects *a posteriori* by multiplying simulated results by a correction factor of 1.26. Following this approach, the dielectric constants of this work were also corrected accordingly, and the adjusted values are also shown in Figs. 2(a) and 2(b). As can be seen, the corrected values align much better with experimental data. The variation of the dielectric constant with

salt addition is well captured by the proposed parameterization, as shown in Fig. 2(c) for NaCl and in Fig. 2(d) for LiCl, where the influence of the OPLS/2016 methanol model is removed by plotting $\Delta\epsilon = (\epsilon(x) - \epsilon(0))/\epsilon(0)$. The dielectric constant for the force field of the Reiser *et al.*⁶⁴ evaluated by Pizio and co-workers⁹⁹ [shown in Fig. 2(a)] takes lower values than our data with similar composition dependence.

The effect of salt addition on viscosity is presented for the three salts in Fig. 3 compared to experimental data.^{101,105,106} As shown, the variation in viscosity with salt addition is well reproduced, except for the CaCl₂ mixture at the highest salt mole fraction, where the simulated value is noticeably higher than the experimental result. For NaCl solutions, the observed discrepancy between simulated and experimental viscosity values can be attributed to a minor limitation of the OPLS/2016 model in representing the viscosity of pure methanol. This difference, however, is not visible in Fig. 3(b) due to the larger scale used in that graph. Overall, the effect of salt addition

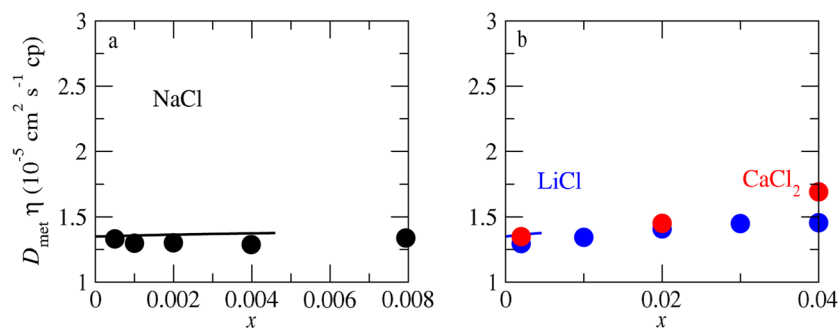


FIG. 5. (a) and (b) The product, $D_{\text{met}}\eta$, is plotted against salt mole fraction, x , at 298.15 K and 1 bar for methanolic solutions of NaCl (black), LiCl (blue), and CaCl₂ (red). Points are the simulation data, and full lines are the experimental data.

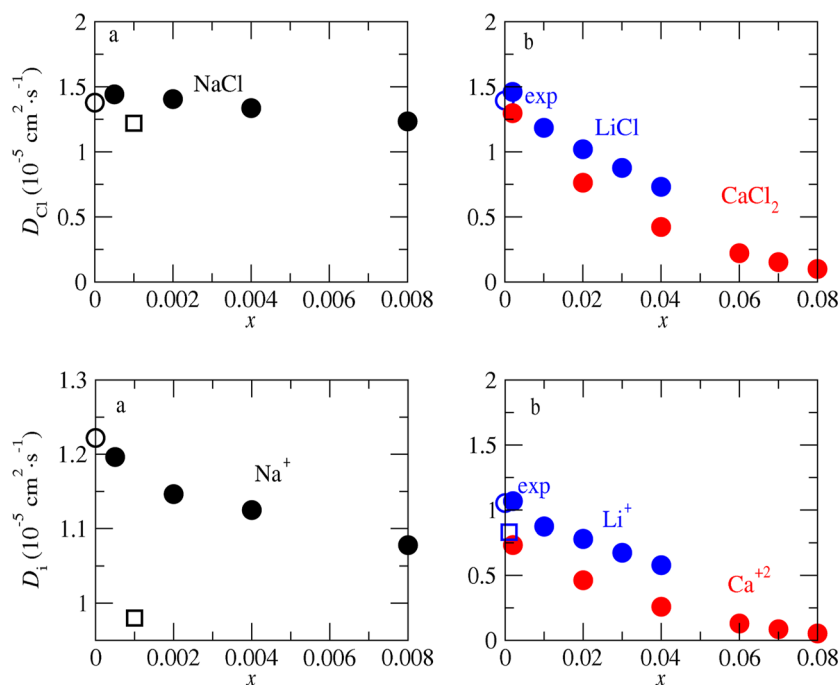


FIG. 6. Self-diffusion coefficient of ion chloride Cl^- , D_{Cl} , plotted against salt mole fraction, x , at 298.15 K and 1 bar for aqueous solutions of (a) NaCl (black) and (b) LiCl (blue) and CaCl_2 (red). Filled circles are the simulation data, empty circles are the experimental data, and empty squares are the simulation data from Reiser *et al.*⁶⁴

FIG. 7. Self-diffusion coefficient of the cation, D_i , plotted against salt mole fraction, x , at 298.15 K and 1 bar for aqueous solutions of (a) NaCl (black) and (b) LiCl (blue) and CaCl_2 (red). Filled circles are the simulation data, empty circles are the experimental data for Na^+ and Li^+ , and empty squares are the simulation data for Na^+ and Li^+ from Reiser *et al.*⁶⁴

on methanol viscosity is well captured. This is more clearly demonstrated in the inset figure, where the influence of the OPLS/2016 methanol model is removed by plotting $\Delta\eta$.

The self-diffusion coefficient of methanol, D_{met} , [panels (a) and (b)] and its variation $\Delta D_{\text{met}} = D_{\text{met}}(x) - D_{\text{met}}(0)$ [panels (c) and (d)] are plotted as functions of salt mole fraction for the three salts studied in this work in Fig. 4. Experimental data¹⁰⁷ are available only for NaCl and LiCl solutions. As observed, the variation of D_{met} with the addition of NaCl or LiCl is well predicted with a small deviation between the experimental and simulated data caused by the OPLS/2016 model's inherent overestimation of the self-diffusion coefficient for pure methanol. This result is particularly important, as the accurate reproduction of the diffusion coefficient variation of water with salt addition is notoriously challenging.^{33,37} For the two monovalent salts, the results are nearly indistinguishable in the range of comparable salt mole fractions. For CaCl_2 solutions, the

self-diffusion coefficients are slightly lower than those of LiCl mixtures. In Fig. 5, the product of the methanol self-diffusion coefficient and the sample viscosity is plotted. According to the Stokes–Einstein relation, this product should remain constant. Simulation results confirm this behavior at low salt mole fractions, but deviations from the rule are observed for mole fractions exceeding 0.01. Nonetheless, the agreement with experimental data is excellent.

The self-diffusion coefficient of the ion Cl^- , D_{Cl} , is presented in Fig. 6 alongside experimental data.^{63,108} In all three cases, the simulated D_{Cl} decreases with increasing salt concentration. Extrapolation of the results for the LiCl and NaCl solutions at infinite dilution appears to be in close agreement with experimental values. A similar agreement is evident in the simulation data reported by Reiser *et al.*⁶⁴ Results for the CaCl_2 solutions were found to be slightly lower than those of LiCl mixtures. The self-diffusion coefficients for the ions Na^+ , Li^+ , and Ca^{2+} are shown in Fig. 7 compared with the available

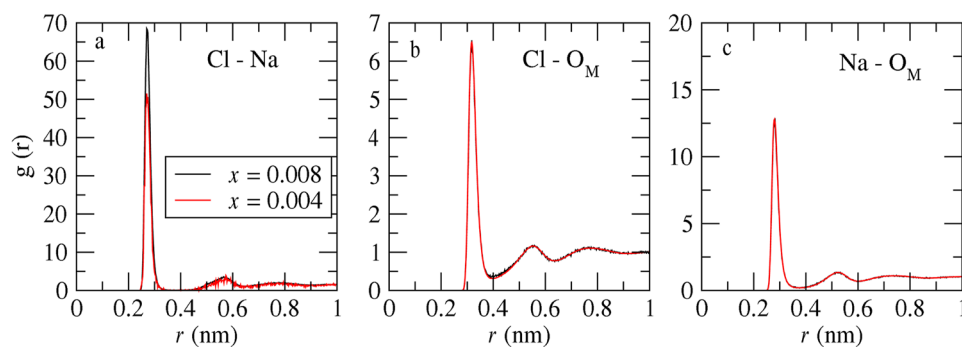


FIG. 8. Radial distributions function, $g(r)$, between (a) Cl^- and Na^+ , (b) Cl^- and O_M , and (c) Na^+ and O_M evaluated for methanolic solutions of NaCl at salt mole fractions $x = 0.004$ (red) and $x = 0.008$ (black).

experimental data.^{63,108} As observed in previous cases, these coefficients decrease with increasing salt concentration. Extrapolations at infinite dilution for the ions Li^+ and Na^+ agree with the experimental data. The results indicate that Na^+ exhibits the highest diffusion coefficients, while Ca^{+2} shows the lowest, with Li^+ falling in between. Notably, the simulation data provided by Reiser *et al.*⁶⁴ are significantly lower than the experimental values in this case.

The radial distribution functions between Cl^- and Na^+ , Cl^- and O_M , and Na^+ and O_M are plotted in Fig. 8 for two methanolic solutions of mole fractions $x = 0.004$ and $x = 0.008$ (experimental solubility). For $g_{\text{Cl}^--\text{Na}^+}(r)$, a strongly pronounced first coordination shell is observed between $r = 0.25$ nm and $r = 0.4$ nm (approximately), with a sharp peak at 0.274 nm, followed by a much softer second coordination shell between $r = 0.4$ nm and $r = 0.65$ nm. This distribution differs significantly from the findings of Pizio and co-workers⁹⁹ at the solubility limit, using alternative models, where the peak of the first shell was notably lower than that of the second shell. Thus, our results indicate a higher probability of finding contact ion pairs (CIPs) than solvent-separated ion pairs (SSIPs), which contrasts with the conclusions of Pizio and co-workers.⁹⁹ The effect of concentration is solely reflected in the height of the first peak, which increases with x . Consequently, the number of CIPs rises from 0.078 at the lower mole fraction to 0.2 at the higher mole fraction (values are provided in Table V). These CIP values exceed those predicted by other models used by Pizio and co-workers, which is attributed to the distinct shape of $g(r)$. Nevertheless, these values align with the rule proposed by Benavides *et al.*⁸⁷ for salt aqueous solutions, which states that the CIP at the solubility limit should be below 0.5 for solubilities less than 11 m (corresponding to a molar salt fraction of ~ 0.165). Regarding the $g_{\text{Cl}^--\text{O}_M}(r)$ and $g_{\text{Na}^+-\text{O}_M}(r)$ radial distribution functions, no significant differences were detected between the lower and the higher salt mole fractions. The first coordination shell for $g_{\text{Cl}^--\text{O}_M}(r)$ spans the interval (0.28, 0.40) nm, whereas for $g_{\text{Na}^+-\text{O}_M}(r)$ it is (0.25, 0.38) nm, approximately. The corresponding coordination numbers were 4.96 and 6.16, respectively. Pizio and co-workers⁹⁹ obtained values for these quantities in the range (5.5–5.9) using different models at a slightly lower concentration $x = 0.001$.

The radial distribution functions between Cl^- and Li^+ , Cl^- and O_M , and Li^+ and O_M are shown in Fig. 9 for two methanolic solutions with mole fractions $x = 0.04$ and $x = 0.20$ (close to the experimental solubility). In this case, the higher mole fraction is five times larger than the lower one, and this provokes appreciable changes in all the analyzed properties. For the $g_{\text{Cl}^--\text{Li}^+}(r)$, an increase

TABLE V. Number of contact ion pairs (CIPs) for salty methanol solutions of salt mole fraction x .

Salt	x	CIP
NaCl	0.003 936	0.078
NaCl	0.007 936	0.20
LiCl	0.040 077	0.21
LiCl	0.20	1.94
CaCl ₂	0.040 077	0.002
CaCl ₂	0.080 037	0.004

in the mole fraction enhances the first peak while diminishing the second peak. The number of CIPs rises significantly, from 0.21 to 1.94 (values are listed in Table V). The rule proposed by Benavides *et al.*⁸⁷ cannot be applied here, as at the solubility limit ($x = 0.25$), the molar fraction exceeds 0.165 (the limit of applicability of the rule, as 11 m for an ionic aqueous solution corresponds to a molar fraction of 0.165). The $g_{\text{Cl}^--\text{O}_M}(r)$ for the lower mole fraction clearly defines the first and second coordination shells. However, at the higher mole fraction, the second shell shifts to shorter distances and appears to overlap with the first one, whose peak is reduced. Consequently, the coordination number decreases from 5.36 to 4.69. For $g_{\text{Li}^+-\text{O}_M}(r)$, changes with concentration are evident in the first peak, which decreases in intensity. The coordination number correspondingly drops from 5.28 to 2.50.

The radial distribution functions between Cl^- and Ca^{+2} , Cl^- and O_M , and Ca^{+2} and O_M are shown in Fig. 10 for two methanolic solutions with mole fractions $x = 0.04$ and $x = 0.08$ (close to experimental solubility). The $g_{\text{Cl}^--\text{Ca}^{+2}}(r)$ function displays an almost undetectable peak in the first coordination shell within the distance range of 0.25–0.32 nm and a pronounced peak in the second coordination shell between 0.32 and 0.5 nm. As a result, the number of contact ion pairs (CIPs) is nearly zero and remains independent of the mole fraction (values are provided in Table V). The $g_{\text{Cl}^--\text{O}_M}(r)$ function shows a more prominent peak in the first coordination shell, with coordination numbers at mole fractions of $x = 0.04$ and $x = 0.08$ being 4.32 and 3.84, respectively. These differences are due to a slight decrease in the peak height and a shift in the position of the first minimum. The $g_{\text{Ca}^{+2}-\text{O}_M}$ function exhibits a strong peak in the first coordination shell, with negligible changes in its shape as a function of mole fraction; the coordination number slightly decreases from 5.99 to 5.97.

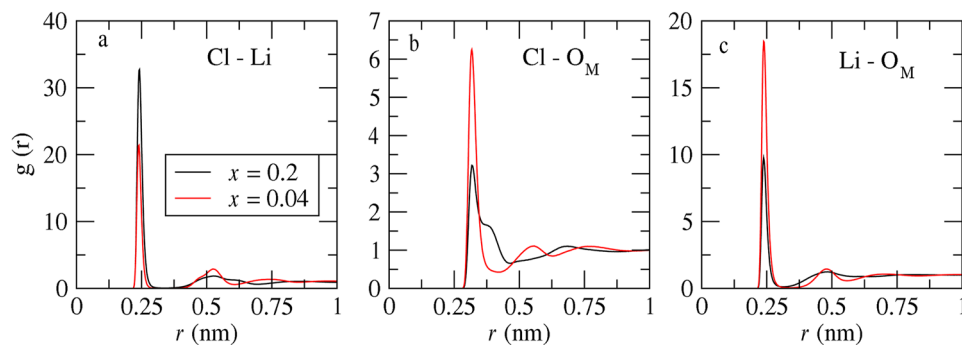


FIG. 9. Radial distributions function, $g(r)$, between (a) Cl^- and Li^+ , (b) Cl^- and O_M , and (c) Li^+ and O_M evaluated for methanolic solutions of LiCl at salt mole fractions $x = 0.04$ (red) and $x = 0.2$ (black).

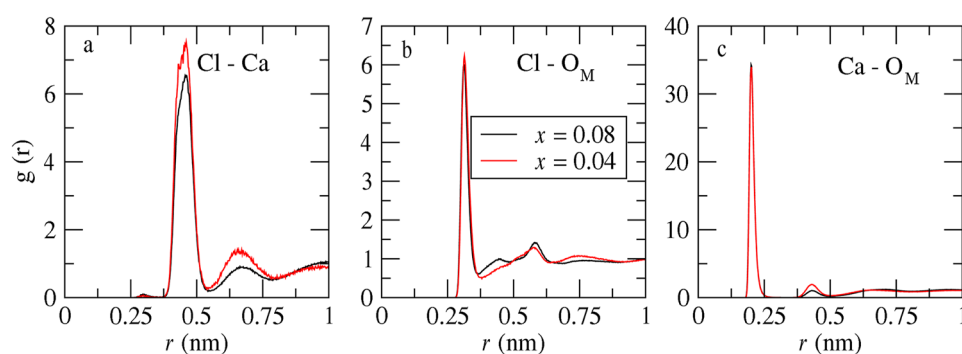


FIG. 10. Radial distributions function, $g(r)$, between (a) Cl^- and Ca^{+2} , (b) Cl^- and O_M , and (c) Ca^{+2} and O_M evaluated for methanolic solutions of CaCl_2 at salt mole fractions $x = 0.04$ (red) and $x = 0.08$ (black). Note that the CIP of this salt is calculated by the integration of the small peak around $r = 0.30$ nm of figure (a).

The position of the first maximum of the radial distribution function between O_M and CH_3 with the anion and cation for a mole fraction of $x = 0.001\,996$ is compared in Table VI with experimental results^{109,110} and simulation data from Reiser *et al.*⁶⁴ The best agreement between our data and experimental results pertains to the r_{max} values for the anion Cl^- , which validates our choice of the LB combining rule for the anion-methanol interaction. Regarding the other quantities, a reasonable level of agreement is observed. The simulation data from Reiser *et al.*⁶⁴ compare with experimental values as our results. For the cation Ca^{+2} , it is noteworthy that the experimental r_{max} value is remarkably small, making it almost impossible to reproduce if the LB combining rule was applied to this interaction (resulting in sigma values of 0.31 and 0.29 nm, respectively). This unusually low value supports our decision to reduce the sigma values between Ca^{+2} and methanol during the fitting process.

Finally, an analysis was conducted to evaluate the ability of the new potential, in combination with the Madrid-2019 model, to predict the densities of the (methanol + water + NaCl) ternary system. Before presenting the results, some details about the Madrid-2019 model and its integration with the new potential in the simulations of the ternary system are provided. As mentioned in the introduction, the Madrid-2019 force field represents water using the TIP4P/2005 model. In this model, water is treated as a rigid body with three masses located at its three atoms: oxygen (O_W) and hydrogens (H_{W1} and H_{W2}). The molecule includes a single LJ interaction site on the oxygen atom, while partial charges are

assigned to the hydrogens, and an M-site is located along the bisector of the $\text{H}_{W1}-\text{O}_W-\text{H}_{W2}$ angle. The geometry and parameters of the water molecule are detailed in Table I. In the Madrid-2019 model, ions are treated as LJ centers with partial charges of $\pm 0.85e$ for monovalent ions and $\pm 1.70e$ for divalent ions. The LJ parameters for the ions are also provided in Table I. Cross-interaction LJ parameters for water-water, water-ion, and ion-ion interactions are summarized in Tables II and III. In the new potential developed for salty methanolic solutions, the charges and LJ parameters for each ion, as well as the ion-ion LJ parameters, are consistent with those in the Madrid-2019 model to ensure compatibility. Therefore, in the ternary system, water-water, water-ion, and ion-ion interactions are taken from the Madrid-2019 model, while methanol-methanol and methanol-ion interactions are those defined in the new potential presented in this work. In addition, LJ cross-interactions between water (TIP4P/2005) and methanol (OPLS/2016) were included, adopting the values reported by one of the authors and collaborators⁸⁶ obtained through fitting of excess thermodynamic properties. These values are also listed in Tables II and III.

Molecular dynamics simulations were performed at 298.15 K and 1 bar for the concentrations and number of components (N_{met} , N_{wat} , and N_{NaCl}) specified in Table VII. These values were selected to closely match the mole fractions for which experimental density data¹¹¹ are available. Our selection corresponds to the water-rich region and the methanol-rich region. For the sake of comparison,

TABLE VI. Position, r_{max} , of the first maximum of the radial distribution function, $g_{XY}(r)$, for the salty methanol solutions of salt mole fraction, x , obtained in this work, simulation literature data (Ref. 64), and experimental data (Refs. 109 and 110).

Salt	Source	x	r_{max} (nm)			
			Cl- O_M	Cl- CH_3	Cation- O_M	Cation- CH_3
NaCl	This work	0.001 996	0.318	0.394	0.278	0.340
	Sim. ⁶⁴	0.002	0.3408	0.4095	0.2212	0.3258
LiCl	This work	0.001 996	0.316	0.390	0.240	0.326
	Sim. ⁶⁴	0.002	0.3408	0.4095	0.2212	0.3258
CaCl ₂	Expt. ¹⁰⁹	0.039	0.316	0.428	0.206	0.270
	This work	0.001 996	0.316	0.392	0.200	0.308
CaCl ₂	Expt. ¹¹⁰	0.039	0.319	0.414	0.239	0.352

TABLE VII. Number of methanol molecules, N_{met} , of water molecules N_{wat} , of cations, N_{+} , and anions, N_{-} , for the methanol + water + NaCl solutions of methanol, water, and NaCl mole fractions, x_{met} , x_{water} , and x_{NaCl} , respectively. Note that $x_{\text{NaCl}} + x_{\text{met}} + x_{\text{water}} = 1$.

x_{met}	x_{water}	x_{NaCl}	N_{met}	N_{wat}	N_{-}	N_{+}
0.890 00	0.106 00	0.004 00	3560	424	16	16
0.896 75	0.102 50	0.000 75	3587	410	3	3
0.897 50	0.100 50	0.002 00	3590	402	8	8
0.092 50	0.902 00	0.005 50	370	3608	22	22
0.102 00	0.895 25	0.002 75	408	3581	11	11
0.102 50	0.881 00	0.016 50	410	3524	66	66
0.000 00	0.999 00	0.001 00	0	4000	4	4
0.000 00	0.998 00	0.002 00	0	4000	8	8
0.000 00	0.996 02	0.003 98	0	4000	16	16
0.000 00	0.992 06	0.007 94	0	4000	32	32
0.000 00	0.984 25	0.015 75	0	4000	64	64

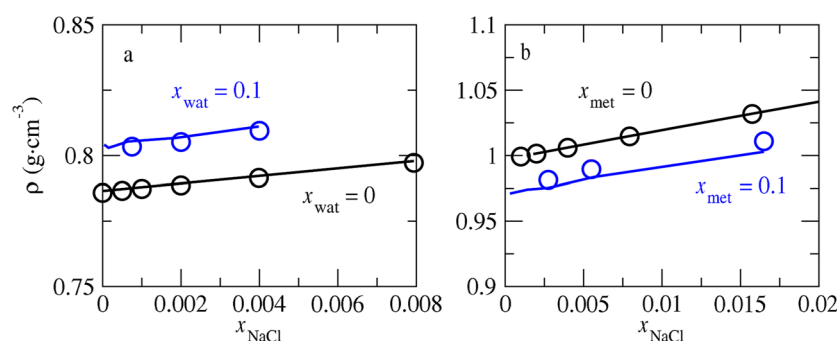


FIG. 11. Density, ρ , as a function of the salt mole fraction, x_{NaCl} , for (x_{NaCl} NaCl + x_{met} methanol + x_{wat} water) at 298.15 K and 1 bar. Simulations (points) and experiments (full line). (a) Methanol rich region and (b) water rich region. Note that $x_{\text{NaCl}} + x_{\text{met}} + x_{\text{wat}} = 1$.

we have also conducted simulations for the binary system water + NaCl with compositions provided in Table VII. The corresponding simulations for the methanol + NaCl system are part of the group of simulations previously described in this work. Figure 11 presents the densities as a function of salt concentration for both binary and ternary systems. At zero salt mole fraction, the influence of adding methanol to water [Fig. 11(a)] or water to methanol [Fig. 11(b)] depends on the LJ cross-interaction parameters between water and methanol. These parameters offer a reasonable description of this effect, as demonstrated in Fig. 11 and in a previous study.⁸⁶ The role of the new potential, combined with the Madrid-2019 model, is to capture the effect of salt addition. As shown, this approach successfully models the salt's influence in the ternary system.

IV. CONCLUSIONS

In this work, an interaction potential for methanolic solutions of salts containing Cl^- , Li^+ , Na^+ , and Ca^{+2} ions is presented. Methanol is modeled using the accurate OPLS/2016 methanol model. Ions are modeled as LJ centers with scaled charges and LJ parameters adopted from the Madrid-2019 potential. The LJ cross parameters between ions were also taken from the Madrid-2019 model, whereas those between ions and the oxygen and methyl sites of the OPLS/2016 model were determined in this study by fitting

to experimental data of the methanolic solutions of LiCl, NaCl, and CaCl_2 . During the fitting procedure, the number of contact pairs, CIP, was carefully controlled to maintain low values, ensuring the avoidance of precipitation at the experimental solubility limit. The accuracy of this parameterization was evaluated by comparison with available experimental data, including density, self-diffusion coefficients for ions and methanol, dielectric constant, and viscosity. The results show that the new parameterization quantitatively reproduces the variation with the salt addition of density, dielectric constant, methanol self-diffusion coefficient, and viscosity. The self-diffusion coefficient of Cl^- , Li^+ , and Na^+ appears to be in agreement with experimental values at infinite dilution. Quantitative discrepancies between simulation properties and experimental data primarily stem from the behavior of the OPLS/2016 model in pure methanol. Regarding structural properties, a reasonable agreement was found between our results of the maximum of the rdf between sites of methanol and both anions and cations and experimental data.

In addition, since this new potential is compatible with the Madrid-2019 model, we performed simulations of salty solutions in methanol–water mixtures at concentrations near those of pure methanol and pure water, respectively. For this purpose, the water–methanol interaction from a previous study was incorporated. Our results demonstrate that the proposed potential quantitatively predicts experimental results. Therefore, the use of scaled charges not only provides reasonable results for ionic aqueous

solutions but also for ionic methanolic solutions and their mixtures with water.

DEDICATION

We would like to dedicate this paper to the memory of Professor Stefan Sokolowski, who sadly passed away in June 2024.¹¹² His work was always robust and inspiring and an example for the younger generations. We have kept in contact and friendship for 35 years. We will miss him.

SUPPLEMENTARY MATERIAL

In the [supplementary material](#), we provide simulated density results for a LiCl methanolic mixture of salt mole fraction $x = 0.04$ at 298.15 K and 1 bar. They were obtained by varying the cross LJ parameters between the sites of methanol and the cation Li^+ . These results allow us to understand our selection of parameters to be fitted or to be constrained to the LB combining rule. We also provide Gromacs *topology* files of the new force field to perform simulations of methanolic solutions of NaCl, LiCl, and CaCl_2 using the OPLS/2016 model for methanol.

ACKNOWLEDGMENTS

The support from the Spanish Ministry of Science and Innovation under Grant Nos. PID2020-115722GB-C22, PID2022-136919NB-C31, and PID2023-147148NB-I00 is greatly acknowledged. The authors want to thank CESGA (Centro de Supercomputación de Galicia) for the use of their computation facilities.

AUTHOR DECLARATIONS

Conflict of Interest

The authors have no conflicts to disclose.

Author Contributions

D. González-Salgado: Data curation (equal); Formal analysis (equal); Funding acquisition (equal); Investigation (equal); Methodology (equal); Software (equal); Writing – original draft (equal); Writing – review & editing (equal). **C. Vega:** Conceptualization (equal); Formal analysis (equal); Funding acquisition (equal); Investigation (equal); Methodology (equal); Writing – original draft (equal); Writing – review & editing (equal).

DATA AVAILABILITY

The data that support the findings of this study are available from the corresponding author upon reasonable request.

REFERENCES

- J. A. Barker and R. O. Watts, *Chem. Phys. Lett.* **3**, 144 (1969).
- A. Rahman and F. H. Stillinger, *J. Chem. Phys.* **55**, 3336 (1971).
- W. L. Jorgensen, J. Chandrasekhar, J. D. Madura, R. W. Impey, and M. L. Klein, *J. Chem. Phys.* **79**, 926 (1983).
- H. J. C. Berendsen, J. P. M. Postma, W. F. van Gunsteren, and J. Hermans, in *Intermolecular Forces*, edited by B. Pullman (Reidel, Dordrecht, 1982), p. 331.
- H. J. C. Berendsen, J. R. Grigera, and T. P. Straatsma, *J. Phys. Chem.* **91**, 6269 (1987).
- J. L. F. Abascal and C. Vega, *J. Chem. Phys.* **123**, 234505 (2005).
- M. Mahoney and W. L. Jorgensen, *J. Chem. Phys.* **115**, 10758 (2001).
- C. Vega and J. L. F. Abascal, *Phys. Chem. Chem. Phys.* **13**, 19663 (2011).
- J. Chandrasekhar, D. C. Spellmeyer, and W. L. Jorgensen, *J. Am. Chem. Soc.* **106**, 903 (1984).
- T. P. Straatsma and H. J. C. Berendsen, *J. Chem. Phys.* **89**, 5876 (1988).
- L. X. Dang, *J. Chem. Phys.* **96**, 6970 (1992).
- D. Beglov and B. Roux, *J. Chem. Phys.* **100**, 9050 (1994).
- P. Cummings, A. Chialvo, and H. Cochran, *Chem. Eng. Sci.* **49**, 2735 (1994).
- D. E. Smith and L. X. Dang, *J. Chem. Phys.* **100**, 3757 (1994).
- B. Roux, *Biophys. J.* **71**, 3177 (1996).
- S. Weerasinghe and P. E. Smith, *J. Chem. Phys.* **119**, 11342 (2003).
- L. Vlcek and I. Nezbeda, *Condens. Matter Phys.* **8**, 261 (2005).
- K. P. Jensen and W. L. Jorgensen, *J. Chem. Theory Comput.* **2**, 1499 (2006).
- J. Alejandre and J.-P. Hansen, *Phys. Rev. E* **76**, 061505 (2007).
- P. J. Lenart, A. Jusufi, and A. Z. Panagiotopoulos, *J. Chem. Phys.* **126**, 044509 (2007).
- I. S. Joung and T. E. I. Cheatham, *J. Phys. Chem. B* **112**, 9020 (2008).
- D. Corradini, M. Rovere, and P. Gallo, *J. Chem. Phys.* **132**, 134508 (2010).
- M. M. Reif and P. H. Hünenberger, *J. Chem. Phys.* **134**, 144104 (2011).
- M. B. Gee, N. R. Cox, Y. Jiao, N. Benteinitis, S. Weerasinghe, and P. E. Smith, *J. Chem. Theory Comput.* **7**, 1369 (2011).
- S. Deublein, J. Vrabec, and H. Hasse, *J. Chem. Phys.* **136**, 084501 (2012).
- F. Moucka, I. Nezbeda, and W. R. Smith, *J. Chem. Theory Comput.* **9**, 5076 (2013).
- J. Kolafa, *J. Chem. Phys.* **145**, 204509 (2016).
- W. R. Smith, I. Nezbeda, J. Kolafa, and F. Moucka, *Fluid Phase Equilib.* **466**, 19 (2018).
- S. Blazquez, I. Zeron, M. Conde, J. Abascal, and C. Vega, *Fluid Phase Equilib.* **513**, 112548 (2020).
- V. M. Trejos, M. de Lucas, C. Vega, S. Blazquez, and F. Gamez, *J. Chem. Phys.* **159**, 224501 (2023).
- S. Blazquez, J. L. Abascal, J. Lagerweij, P. Habibi, P. Dey, T. J. Vlugt, O. A. Moulτος, and C. Vega, *J. Chem. Theory Comput.* **19**, 5380 (2023).
- S. Blazquez, C. Vega, and M. Conde, *J. Mol. Liq.* **383**, 122031 (2023).
- S. Blazquez, M. M. Conde, and C. Vega, *J. Chem. Phys.* **158**, 054505 (2023).
- F. Gamez, L. Sedano, S. Blazquez, J. Troncoso, and C. Vega, *J. Mol. Liq.* **377**, 121433 (2023).
- L. F. Sedano, S. Blazquez, E. G. Noya, C. Vega, and J. Troncoso, *J. Chem. Phys.* **156**, 154502 (2022).
- S. Koneshan, J. C. Rasaiah, R. M. Lynden-Bell, and S. H. Lee, *J. Phys. Chem. B* **102**, 4193 (1998).
- J. S. Kim, Z. Wu, A. R. Morrow, A. Yethiraj, and A. Yethiraj, *J. Phys. Chem. B* **116**, 12007 (2012).
- A. Z. Panagiotopoulos, *J. Chem. Phys.* **153**, 010903 (2020).
- S. Blazquez, M. M. Conde, J. L. F. Abascal, and C. Vega, *J. Chem. Phys.* **156**, 044505 (2022).
- M. Jorge and L. Lue, *J. Chem. Phys.* **150**, 084108 (2019).
- A. W. Milne and M. Jorge, *J. Chem. Theory Comput.* **15**, 1065 (2019).
- I. V. Leontyev and A. A. Stuchebrukhov, *J. Chem. Phys.* **130**, 085102 (2009).
- I. V. Leontyev and A. A. Stuchebrukhov, *J. Chem. Theory Comput.* **6**, 3153 (2010).
- I. V. Leontyev and A. A. Stuchebrukhov, *J. Chem. Theory Comput.* **6**, 1498 (2010).
- I. V. Leontyev and A. A. Stuchebrukhov, *Phys. Chem. Chem. Phys.* **13**, 2613 (2011).
- I. V. Leontyev and A. A. Stuchebrukhov, *J. Chem. Theory Comput.* **8**, 3207 (2012).
- I. V. Leontyev and A. A. Stuchebrukhov, *J. Chem. Phys.* **141**, 014103 (2014).
- V. Kostal, P. Jungwirth, and H. Martinez-Seara, *J. Phys. Chem. Lett.* **14**, 8691 (2023).

- ⁴⁹T. Martinek, E. Duboue-Dijon, S. Timr, P. E. Mason, K. Baxova, H. E. Fischer, B. Schmidt, E. Pluharova, and P. Jungwirth, *J. Chem. Phys.* **148**, 222813 (2018).
- ⁵⁰E. Wernersson and P. Jungwirth, *J. Chem. Theory Comput.* **6**, 3233 (2010).
- ⁵¹M. Kohagen, P. E. Mason, and P. Jungwirth, *J. Phys. Chem. B* **118**, 7902 (2014).
- ⁵²M. Kohagen, P. E. Mason, and P. Jungwirth, *J. Phys. Chem. B* **120**, 1454 (2016).
- ⁵³E. Duboue-Dijon, P. E. Mason, H. E. Fischer, and P. Jungwirth, *J. Phys. Chem. B* **122**, 3296 (2018).
- ⁵⁴Z. R. Kann and J. L. Skinner, *J. Chem. Phys.* **141**, 104507 (2014).
- ⁵⁵I. M. Zeron, J. L. F. Abascal, and C. Vega, *J. Chem. Phys.* **151**, 134504 (2019).
- ⁵⁶W. L. Jorgensen, *J. Phys. Chem.* **90**, 1276 (1986).
- ⁵⁷M. Haughney, M. Ferrario, and I. R. McDonald, *J. Phys. Chem.* **91**, 4934 (1987).
- ⁵⁸M. E. van Leeuwen and B. Smith, *J. Phys. Chem.* **99**, 1831 (1995).
- ⁵⁹T. Schnabel, A. Srivastava, J. Vrabec, and H. Hasse, *J. Phys. Chem. B* **111**, 9871 (2007).
- ⁶⁰D. Gonzalez-Salgado and C. Vega, *J. Chem. Phys.* **145**, 034508 (2016).
- ⁶¹S. Chowdhuri and A. Chandra, *J. Chem. Phys.* **124**, 084507 (2006).
- ⁶²S. Chowdhuri and S. K. Pattanayak, *J. Mol. Liq.* **180**, 172 (2013).
- ⁶³P. Kumar, S. R. Varanasi, and S. Yashonath, *J. Phys. Chem. B* **117**, 8196 (2013).
- ⁶⁴S. Reiser, M. Horsch, and H. Hasse, *J. Chem. Eng. Data* **60**, 1614 (2015).
- ⁶⁵E. Hawlicka and D. Swiatla-Wojcik, *Phys. Chem. Chem. Phys.* **2**, 3175 (2000).
- ⁶⁶E. Hawlicka and D. Swiatla-Wojcik, *J. Mol. Liq.* **98–99**, 357 (2002).
- ⁶⁷E. Hawlicka and D. Swiatla-Wojcik, *J. Phys. Chem. A* **106**, 1336 (2002).
- ⁶⁸E. Hawlicka and D. Swiatla-Wojcik, *J. Chem. Phys.* **119**, 2206 (2003).
- ⁶⁹P. Kumar, A. D. Kulkarni, and S. Yashonath, *J. Phys. Chem. B* **119**, 10921 (2015).
- ⁷⁰R. W. Impey, M. Sprik, and M. L. Klein, *J. Am. Chem. Soc.* **109**, 5900 (1987).
- ⁷¹D. Marx, K. Heinzinger, G. Pálkás, and I. Bakó, *Z. Naturforsch. A* **46**, 887 (1991).
- ⁷²G. Sesé, E. Guàrdia, and J. A. Padró, *J. Chem. Phys.* **105**, 8826 (1996).
- ⁷³G. Sesé and J. Padró, *J. Chem. Phys.* **108**, 6347 (1998).
- ⁷⁴H. J. Strauch and P. T. Cummings, *Fluid Phase Equilib.* **86**, 147 (1993).
- ⁷⁵E. Hawlicka and D. Swiatla-Wojcik, *Chem. Phys.* **195**, 221 (1995).
- ⁷⁶E. Hawlicka and D. Swiatla-Wojcik, *Chem. Phys.* **232**, 361 (1998).
- ⁷⁷T. Długoborski, E. Hawlicka, and D. Swiatla-Wojcik, *J. Mol. Liq.* **85**, 97 (2000).
- ⁷⁸S. Chowdhuri and A. Chandra, *J. Chem. Phys.* **123**, 234501 (2005).
- ⁷⁹E. Owczarek, M. Rybicki, and E. Hawlicka, *J. Phys. Chem. B* **111**, 14271 (2007).
- ⁸⁰E. Owczarek, M. Rybicki, and E. Hawlicka, *Chem. Phys.* **363**, 78 (2009).
- ⁸¹M. Rybicki and E. Hawlicka, *Chem. Phys.* **400**, 79 (2012).
- ⁸²M. Rybicki and E. Hawlicka, *J. Mol. Liq.* **196**, 300 (2014).
- ⁸³M. Kelley, A. Donley, S. Clark, and A. Clark, *J. Phys. Chem. B* **119**, 15652 (2015).
- ⁸⁴S. Keshri, A. Sarkar, and B. Tembe, *J. Supercrit. Fluids* **103**, 61 (2015).
- ⁸⁵M. C. Sanchez, J. Gujt, S. Sokolowski, and O. Pizio, *Condens. Matter Phys.* **21**, 23601 (2018).
- ⁸⁶D. González-Salgado, K. Zemánková, E. G. Noya, and E. Lomba, *J. Chem. Phys.* **144**, 184505 (2016).
- ⁸⁷A. L. Benavides, M. A. Portillo, J. Abascal, and C. Vega, *Mol. Phys.* **115**, 1301 (2017).
- ⁸⁸M. P. Allen and D. J. Tildesley, *Computer Simulation of Liquids* (Oxford University Press, 1987).
- ⁸⁹D. Frenkel and B. Smit, *Understanding Molecular Simulation* (Academic Press, London, 1996).
- ⁹⁰D. Van Der Spoel, E. Lindahl, B. Hess, G. Groenhof, A. E. Mark, and H. J. C. Berendsen, *J. Comput. Chem.* **26**, 1701 (2005).
- ⁹¹S. Nosé, *Mol. Phys.* **52**, 255 (1984).
- ⁹²W. G. Hoover, *Phys. Rev. A* **31**, 1695 (1985).
- ⁹³M. Parrinello and A. Rahman, *J. Appl. Phys.* **52**, 7182 (1981).
- ⁹⁴U. Essmann, L. Perera, M. L. Berkowitz, T. Darden, H. Lee, and L. G. Pedersen, *J. Chem. Phys.* **103**, 8577 (1995).
- ⁹⁵M. Li, D. Constantinescu, L. Wang, A. Mohs, and J. Gmehling, *Ind. Eng. Chem. Res.* **49**, 4981 (2010).
- ⁹⁶S. P. Pinho and E. A. Macedo, *J. Chem. Eng. Data* **50**, 29 (2005).
- ⁹⁷O. Rodinkov, G. Zhuravlyova, E. Vaskova, and I. A. Platonov, *Anal. Methods* **7**, 458 (2015).
- ⁹⁸I.-C. Yeh and G. Hummer, *J. Phys. Chem. B* **108**, 15873 (2004).
- ⁹⁹M. Cruz Sanchez, H. Dominguez, and O. Pizio, "On the properties of methanolic NaCl solution by molecular dynamics simulations," *Condens. Matter Phys.* **23**, 23602 (2020).
- ¹⁰⁰O. V. Eliseeva, V. V. Golubev, A. A. Dyshin, M. G. Kiselev, and G. A. Al'per, *Russ. J. Phys. Chem.* **80**, 205 (2006).
- ¹⁰¹A. Wahab and S. Mahiuddin, *J. Chem. Eng. Data* **46**, 1457 (2001).
- ¹⁰²P. Winsor IV and R. H. Cole, *J. Phys. Chem.* **86**, 2491 (1982).
- ¹⁰³C. Vega, *Mol. Phys.* **113**, 1145 (2015).
- ¹⁰⁴S. Blazquez, L. F. Sedano, and C. Vega, *J. Chem. Phys.* **161**, 044505 (2024).
- ¹⁰⁵L. Werblan, A. Rotowska, and S. Minc, *Electrochim. Acta* **16**, 41 (1971).
- ¹⁰⁶O. Tower, *J. Am. Chem. Soc.* **38**, 833 (1916).
- ¹⁰⁷E. Hawlicka, *Ber. Bunsenges. Phys. Chem.* **88**, 1002 (1984).
- ¹⁰⁸E. Hawlicka, *Z. Naturforsch. A* **41**, 939 (1986).
- ¹⁰⁹T. Megyes, T. Radnai, T. Grósz, and G. Pálkás, *J. Mol. Liq.* **101**, 3 (2002).
- ¹¹⁰T. Megyes, S. Bálint, I. Bakó, T. Grósz, T. Radnai, and G. Pálkás, *Chem. Phys.* **327**, 415 (2006).
- ¹¹¹T. Guetachew, S. Ye, I. Mokbel, J. Jose, and P. Xans, *J. Solution Chem.* **25**, 895 (1996).
- ¹¹²O. Pizio, A. Patrykiewicz, C. Vega, L. Pusztai, J. Illytskyi, T. Patsahan, and A. Trokhymchuk, *Condens. Matter Phys.* **27**, 37001 (2024).